Quantum transport in topological mesoscopic ring structures

1998 J. Phys.: Condens. Matter 10 1065

(http://iopscience.iop.org/0953-8984/10/5/014)

J. Phys.: Condens. Matter **10** (1998) 1065–1077. Printed in the UK PII: S0953-8984(98)85680-4

Quantum transport in topological mesoscopic ring structures

Yan Chen†, Shi-Jie Xiong†‡ and S N Evangelou§

† Solid State Microstructure Laboratory and Department of Physics, Nanjing University, Nanjing 210008, People's Republic of China

‡ China Centre of Advanced Science and Technology (World Laboratory), PO Box 8730, Beijing 100080, People's Republic of China

§ Department of Physics, University of Ioannina, Ioannina 45 110, Greece

Received 30 June 1997, in final form 27 October 1997

Abstract. We have studied the electronic transport properties of various topological mesoscopic rings which consist of several variable-size chains joined at their ends to form ideal single-channel leads. An enhancement of the transmission coefficient is obtained when the chain lengths are randomly distributed, due to the suppression of interchain interference, and, in the presence of magnetic flux, periodic magnetoconductance oscillations are also shown. A single impurity changes the magneto-oscillation pattern drastically, while for more impurities placed at random the periodic magnetoconductance oscillations survive. Finally, the introduction of a transverse link between the chains destroys the bridge-arc shape of the transmission versus energy curves obtained in the absence of such a link.

1. Introduction

In recent years electronic transport properties of mesoscopic structures have been extensively investigated both experimentally and theoretically [1–3]. This is not only due to recent advances made in microtechnology which allowed the fabrication of such microstructures but also to the strong need for building microelectronic devices for technological purposes. Most device concepts rely on quantum interference phenomena [4, 5] which are generally expected to wash out for larger devices, due to the fact that only for small enough sizes and at sufficiently low temperatures does the quantum wave function maintain phase coherence across the sample. In the quantum coherent case, idealized samples behave as electron waveguides, and the electronic transport properties are solely determined by the geometry of the conductor, as well as the topology of the impurity distributions [6, 7].

Quantum transport in two-arm mesoscopic rings has attracted considerable attention since it represents an experimental realization of the Aharonov–Bohm (AB) effect [8–11]. Waves propagating from left to right along the two branches of a ring suffer phase shifts which lead to constructive or destructive interference patterns at the right-hand contact. Moreover, the flux-dependent conductance is ϕ_0-periodic, with ϕ_0 the flux quantum, as shown by one-dimensional (1D) disordered metallic rings with a magnetic field [12]. The electronic transport through extended AB rings which consist of more than two chains has also recently been studied [13]. In a perfect multi-arm ring connected to single-channel ideal leads, the conduction band splits into many sub-bands due to the geometry of the electrodes, and the magnetoconductance shows a very complicated oscillating behaviour in

0953-8984/98/051065+13$19.50

comparison with the common two-arm-ring AB effect. Moreover, in the limit of large chain numbers the conductance rapidly approaches zero for most energies, and interesting wave blocking or 'localization' is obtained, due to quantum interference rather than disorder [13].

In the present paper we study the quantum transport properties through similar mesoscopic ring geometries made of several chains with fixed or random lengths, complementing and extending the previous results [13]. For structures with random chain lengths we obtain average transmission enhancement due to the suppression of interchain interference. In the presence of a magnetic flux we still observe periodic magnetoconductance oscillations with increased average conductance when the variance of the random chain length distribution increases. We have also studied doped multi-chain structures by adding one or more impurities. The presence of a single impurity is shown to change drastically the magneto-oscillation pattern, while for many impurities the magnetoconductance still exhibits periodic oscillations. Moreover, the introduction of a transverse link between the chains is shown to destroy the bridge-arc shape of the transmission versus energy diagram obtained without such a link [13].

In section 2 we introduce the basic model and the formulae which are used in this paper. The results obtained and their analysis are described in section 3. Finally, the last section, section 4, is devoted to a summary of our conclusions.

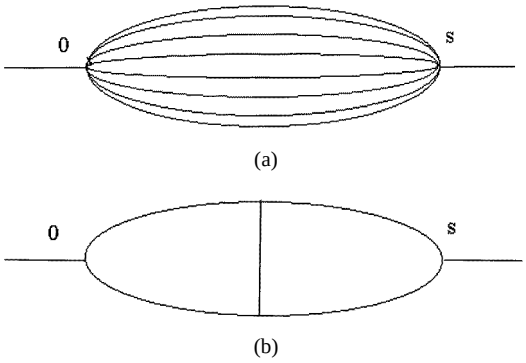

Figure 1. A schematic picture of the single-lead topological systems studied: (a) a singly connected multi-arm structure, and (b) a doubly connected two-arm structure.

2. The model and formulae

The geometry of the topological structures studied shown in figure 1(a) is a ring with many chains connected to perfect left-hand and right-hand single-channel leads at the nodes 0 and s. The transmission through this system can be studied by considering a plane wave incident from the right so that the corresponding wave function coefficients in the ideal leads can be written as $a_j = \mathrm{e}^{-\mathrm{i}kj}$, for $j \leqslant 0$, and $a_j = A\mathrm{e}^{-\mathrm{i}k(j-s)} + R\mathrm{e}^{\mathrm{i}k(j-s)}$, for $j \geqslant s$, where $k = \cos^{-1}(E/2)$ is the wave vector corresponding to the pure chain lead, E the incident energy, and A (R) the amplitude of the incident (reflected) wave. We take unit transmission amplitude and assume narrow enough width of the structure considered compared to its length that experimentally our system corresponds to a network of high-mobility narrow quantum wires where only the lower sub-band is sufficiently populated. In this picture the branches of the ring can be safely treated as 1D channels.

In the absence of inelastic scattering, the electronic transmission through the multi-chain

ring can be described by the tight-binding Hamiltonian

$$H = \sum_{\alpha=1}^{N} \sum_{i=1}^{N_\alpha} \varepsilon_{\alpha,i} c^{\dagger}_{\alpha,i} c_{\alpha,i} - t_0 \sum_{\alpha=1}^{N} \left(c^{\dagger}_{0} c_{\alpha,1} + \mathrm{e}^{\mathrm{i}\phi_\alpha} c^{\dagger}_{\alpha,N_\alpha} c_s + \sum_{i=1}^{N_\alpha - 1} c^{\dagger}_{\alpha,i} c_{\alpha,i+1} + \mathrm{HC} \right) \tag{1}$$

where $c_{\alpha,i}$ ($c^{\dagger}_{\alpha,i}$) annihilates (creates) an electron on site i of chain α, the two lead node sites are labelled by 0 and s, N_α is the number of sites in the αth chain (excluding the nodes 0 and s), and N is the total number of chains. The Hamiltonian includes both diagonal disorder and electrostatic bias applied in the transverse direction, taken into account via the on-site energy $\epsilon_{\alpha,i}$. We assume that the applied bias generates a potential difference only between the neighbouring $(N-1)$th and Nth chains in the present geometry. The significant point which allows a simple numerical treatment of the problem is that the chains are connected to form ideal single-channel leads at their ends 0 and s. We can also make the convenient choice of the gauge of the vector potential to affect only the phase of the wave functions at the hopping bonds between the right-hand chain ends (sites N_α, $\alpha = 1, 2, \ldots, N$) and the right-hand node s. This choice for the magnetic field is expressed via the third term of equation (1), with the phase difference $\phi_\alpha - \phi_{\alpha-1}$ proportional to the flux HW_α, $\alpha = 2, 3, \ldots, N$, with H the strength of the field, and W_α the area enclosed by the αth and the $(\alpha-1)$th chains. For convenience, we choose the phase of the first chain $\phi_1 = 0$ and the hopping strength $t_0 = 1$, which defines the energy unit throughout the paper.

The boundary conditions at the two nodes 0 and s present a serious difficulty which can be solved, making Griffith's choice, by introducing the requirements that the wave functions are single valued and the current density is conserved (Kirchhoff's law) [14]. The wavefunction component for the jth site of the αth chain reads

$$\psi_{\alpha,j} = A_\alpha \mathrm{e}^{\mathrm{i}(k+\theta_\alpha)j} + B_\alpha \mathrm{e}^{-\mathrm{i}(k-\theta_\alpha)j} \tag{2}$$

where $\theta_\alpha = \phi_\alpha / N_\alpha$, and the requirements of single-valued functions and continuity at 0, s lead to the equations

$$\psi_{1,0} = \psi_{2,0} = \cdots = \psi_{N,0} \qquad \psi_{1,N_1+1} = \psi_{2,N_2+1} = \cdots = \psi_{N,N_N+1} \tag{3}$$

at the two node points 0 and $s = N_\alpha + 1, \alpha = 1, 2, \ldots, N$. A numerical solution of equations (1)–(3) is the central point of the present work. In the absence of impurities, there are $2N$ unknown coefficients; hence equation (3) is complete at the two nodes, and the wave function can be readily evaluated for all sites involved in the structure. The transmission coefficient $T = 1/|A|^2$ measures the transparency of the system and allows one to obtain the E-dependent dimensionless conductance $\sigma(E) = T(E)$ from Landauer's formula [15]. In reference [13] an analytical formula was possible for such multi-arm mesoscopic rings, also with an imposed flux or electrostatic potential, but in the absence of impurities, diagonal disorder, and transverse crosslinks.

It may also be worth mentioning that the commonly accepted symmetry of the transmission coefficient, $t(E) = t(-E)$ without magnetic field and/or disorder, due to the electron–hole symmetry, although rarely found experimentally was satisfied in our case when all the chains had either even or odd numbers of sites. If some chains have even and others odd numbers of sites, $t(E) \neq t(-E)$. This can be checked from equations (1)–(3) by observing that a projection $E \to -E$ corresponds to $\mathrm{e}^{\mathrm{i}kN_\alpha} \to (-1)^{N_\alpha} \mathrm{e}^{-\mathrm{i}kN_\alpha}$. After some algebra we can show that $t(E) = t(-E)$ only if all of the chains have even (or all have odd) numbers of sites; otherwise $t(E) \neq t(-E)$, in agreement with our numerical findings. The asymmetry of the transmission coefficient is due to the special geometry of the structure considered. The influence of the number of atoms on the symmetry of

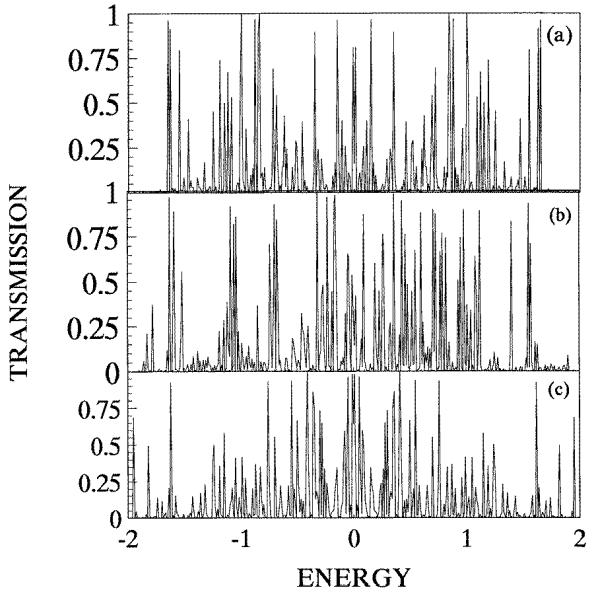

Figure 2. The transmission coefficient as a function of energy for structures which consist of ten chains with random lengths uniformly distributed in $[L-\delta L, L+\delta L]$, with $L = 1000$, the incident-electron energy fixed at $E = 1.1$, and obtained by taking the ensemble average over 100 random configurations. (a) $\delta L = 0$, (b) $\delta L = 100$, and (c) $\delta L = 500$.

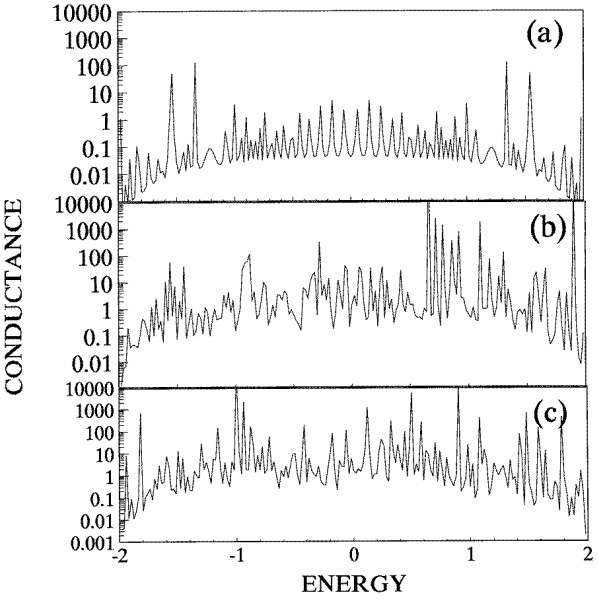

Figure 3. The conductance as a function of energy for structures each composed of a hundred chains with lengths uniformly distributed in $[L-\delta L, L+\delta L]$, $L = 1000$, the incident-electron energy fixed at $E = 1.1$, and the ensemble average taken over 200 random configurations. (a) $\delta L = 0$, (b) $\delta L = 10$, and (c) $\delta L = 100$.

the magnetoconductance was pointed out in reference [16], where a similar conclusion was reached for a mesoscopic ring subjected to magnetic flux. Our study generalizes this finding for the many-chain topological structures, also in the presence of impurities.

3. Numerical results and discussion

We present results obtained by varying the number of chains involved in the structure as well as their lengths, and show that the splitting of the band into many sub-bands can seriously modify the transport properties of the system.

3.1. Chains of variable lengths

Equation (10) of reference [13] gives an exact expression for the transmission coefficient for a multi-chain Aharonov–Bohm ring with arbitrary chain lengths in the absence of impurities. In figure 2 we plot the energy-dependent transmission coefficient for a ten-chain structure with various values for the variance of the random length distribution. We observe average transmission enhancement when the randomness in the chain lengths becomes stronger. The magnetoconductance pattern is shown in figure 3 for structures each composed of a higher number of chains (100), and for fixed chain lengths (figure 3(a)) the curves show the usual principal and secondary maxima [13]. For random chain lengths, periodic oscillations can be still observed with enhanced conductance on average. The higher average transmission obtained can be attributed to the suppression of interference, since variations in the chain lengths cause the phases of the waves for different chains to become uncorrelated. In the presence of magnetic flux the magnetoconductance displays similar behaviour.

3.2. Chains with few impurities

A single defect added at any site of the multi-chain structure can significantly modify the band obtained. In figure 4(a), transmission zeros can be seen in the absence of magnetic field and impurities. A single impurity added at the centre of one of the chains is shown to strongly modify the transmission pattern obtained (figure 4(b)). Physically, this can be understood on the basis of the total transmission probability which is related to the interference pattern via a sum over all paths, starting from node 0 and ending at node s. In the presence of one (figure 4(b)) or more (figure 4(c)) impurities the paths are strongly influenced by the impurities; hence the interference in the sum changes and the transmission probability becomes extremely sensitive to the presence of impurities.

In figure 5 we consider the evolution of the band structure as a function of the magnetic flux ϕ, and we can see oscillations with period $9\phi_0$ [13]. This periodicity does not seem to change in the presence of disorder, in agreement with reference [13], where chain length variations were also considered. We have previously observed [13] that the period of magnetic oscillation for an N-chain loop is the sum of the periods of the loops formed by nearest-neighbour chains. The period in the present case is also $(N-1)\phi_0$ which is also the sum of all the loop periods. Moreover, in figure 5(a) the magnetic field is shown to induce destructive interference effects, with many ϕ-values with zero transmission. In figures 5(b) and 5(c) the presence of impurities is seen to erase these zero-transmission points, causing a remarkable change of the interference pattern obtained. We also notice that the eight subsidiary maxima in the absence of disorder (figure 5(a)) reduce to seven in the presence of one impurity. Generally, for an N-chain ring structure without impurities, the magneto-oscillation periodicity and the number of subsidiary maxima are $N-1$ and

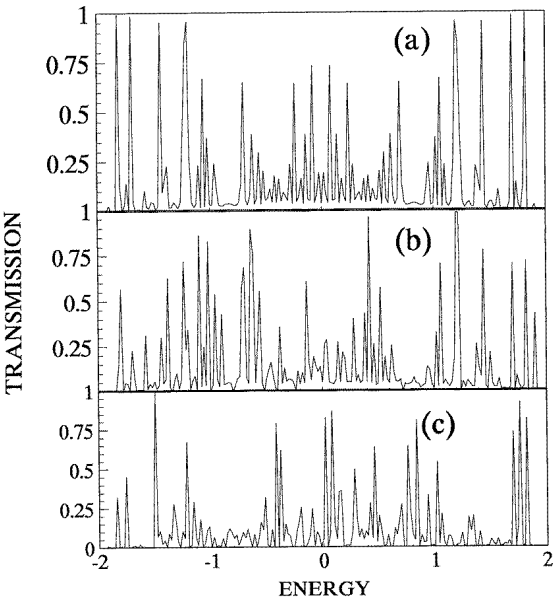

Figure 4. The transmission coefficient versus energy for a ten-chain structure also with impurities. The site energy of the impurity is equal to 3.0 and the length of the chains is 2000. (a) No impurity, (b) one impurity at the centre of one chain, and (c) four impurities randomly distributed for a single configuration.

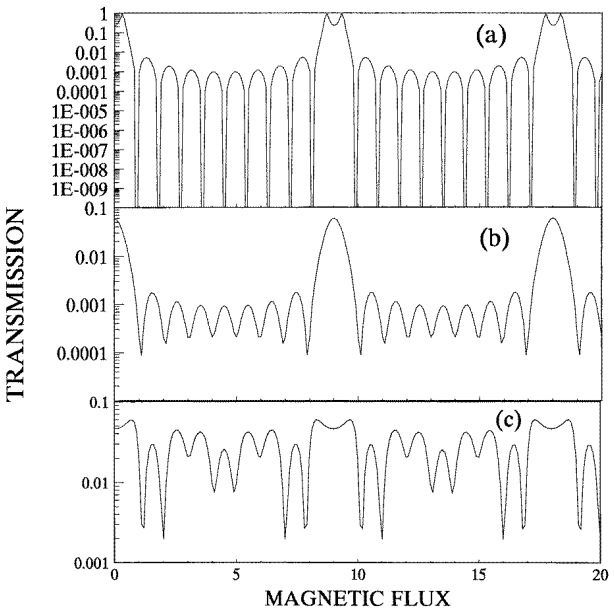

Figure 5. The transmission coefficient versus the magnetic flux threaded in a structure with impurities; the rest of the parameters are as in figure 4, and energy $E = 1.1$. (a) No impurity, (b) one impurity at the centre of one chain, and (c) four impurities randomly distributed for a single configuration.

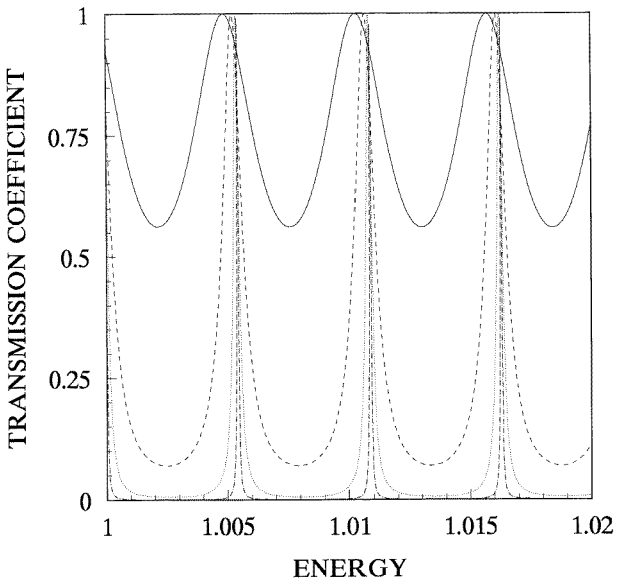

Figure 6. The transmission coefficient versus the energy for structures composed of various numbers of chains N with the chain length fixed to 1000, for $N = 2$, (solid line), $N = 6$ (dashed line), $N = 20$ (dotted line), and $N = 80$ (dashed–dotted line).

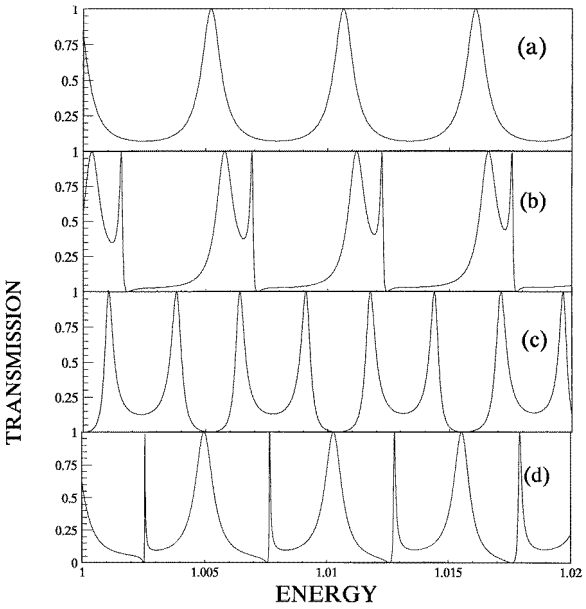

Figure 7. The transmission coefficient versus the electron energy for various electrostatic potentials with chain lengths equal to 1000. (a) $V = 0$, (b) $V = 0.05$, (c) $V = 0.1$, and (d) $V = 0.2$.

$N - 2$, respectively [13]. This may be due to changes of interference caused by impurity scattering. In the presence of a single impurity, the magneto-oscillation periodicity does not

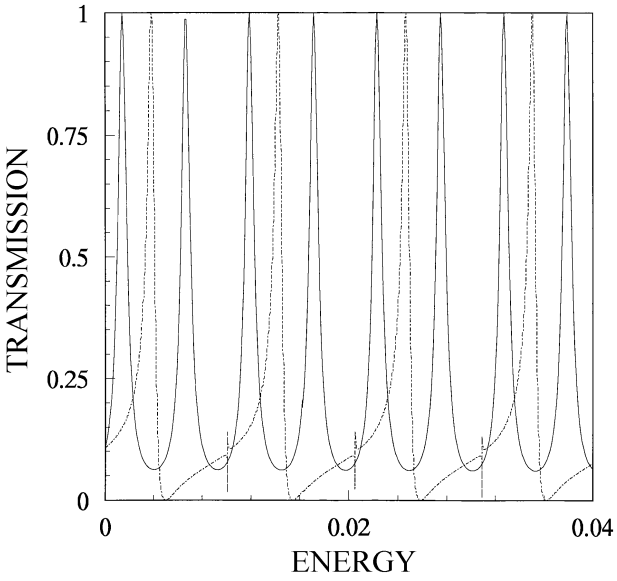

Figure 8. A comparison between energy-induced and electrostatic AB oscillations, with the rest of the parameters as in figure 6. The transmission versus the electron energy (solid line), and the transmission versus the electrostatic potential (dashed line).

change but the number of subsidiary maxima decreases from $N-2$ to $N-3$, while more impurities give a rather complicated plot (figure 5(c)).

3.3. Energy- and voltage-induced oscillations

We have investigated energy- and voltage-induced oscillations of the multi-arm structure considered. Firstly, in figure 6 we consider the energy-induced oscillation where the conductance curves show periodic oscillations depending on the electron energy E. Moreover, the conductance exhibits peaks when E coincides with an eigen-energy of the system, and for large numbers of chains the band splits into minibands with sharper conductance peaks. The physical reason for this behaviour is the lack of propagation, or 'localization', for the majority of states, in this case due to the band splitting, despite the absence of disorder and/or interchain coupling. This is again a result of quantum interference, except for the resonance points where the transmission takes a simple resonant form (figure 6). For more chains ($N = 80$) the ratio between the periodicity and the width of the resonance peak found is nearly one hundred.

We have also studied the energy-induced oscillations due to the influence of an electrostatic potential applied in the transverse direction. In figure 7 we show the conductance for various potential differences between one chain and the others. The modulation of the conductance oscillations by the electrostatic potential arises from variations in the relative phase shifts. If the voltage increases, the periodic behaviour remains unchanged, although the transmission pattern may exhibit a different shape. A vanishingly small voltage gives a bridge-arc shape of the conductance in the bulk band region [13], while a higher voltage modifies the position and the sharpness of peaks, and there are a few new sharp peaks.

In figure 8 we observe the period ϕ_E of the energy-induced oscillations to be exactly double the voltage-induced oscillation period ϕ_V, which can be deduced from the analytical expression for the conductance (equation (10) of [13]). In this case the periodicities occur at $\Delta k\, L = n\pi$, where n is any integer. The voltage-induced oscillations arise from phase shifts in the different paths which vary as a function of the incident-electron energy [17]. The electrostatic phase shift is given by $\Delta\phi = (k' - k)L$, where $k = \cos^{-1}(E/2)$ and $k' = \cos^{-1}((E+V)/2)$. Thus, if the period of the voltage-induced oscillation is $\Delta\phi = 2n\pi$, the corresponding energy-induced oscillation period is $\Delta\phi = 4n\pi$.

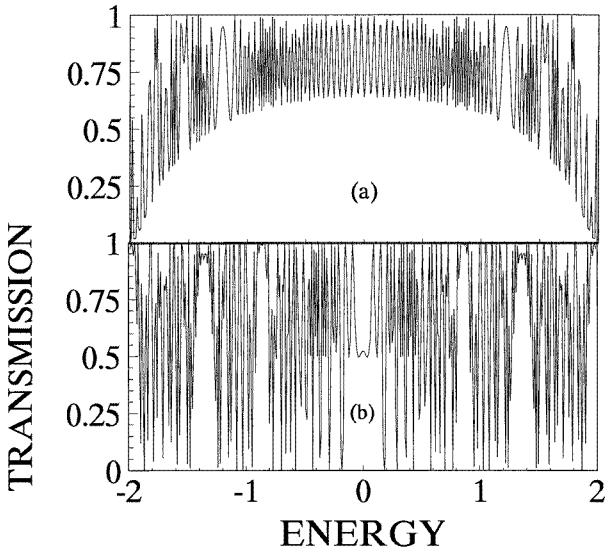

Figure 9. A comparison of the transmission for singly connected AB rings and that for doubly connected AB rings. (a) A singly connected AB ring with chain lengths equal to 2000, and (b) a doubly connected AB ring with each arm segment equal to 1000 and rung length 1000.

3.4. Doubly connected AB rings

We have also examined the conductance of doubly connected structures (figure 1(b)) assuming, for simplicity, perfect ballistic transport. The classical counterpart of a doubly connected ring corresponds to a Wheatstone bridge circuit which, if balanced, has a conductance independent of the variation of the ring resistance. The quantum case is clearly much more complicated. In figure 9 we plot numerical results for the transmission band in this case, and for doubly connected rings the bridge-arc shape exhibited for singly connected two-arm AB rings is completely destroyed. In figure 9(b) we can see transmission zeros due to destructive interference. In the doubly connected ring the additional two nodes (figure 1(b)) provide additional destructive interference at the exit. In figure 10 we expand figure 9 in greater detail and report oscillations with elegant periodicities. It is interesting to notice that the periodicity of (a) is half that of (b), that of (b) half that of (c), and that of (c) a quarter that of (d). The improved periodicity arises from the increase in the node number and the variations in the chain lengths.

In our study of doubly connected rings we have also considered the influence of the rung length on the magnetoconductance oscillations. The rung length is defined as the crossing

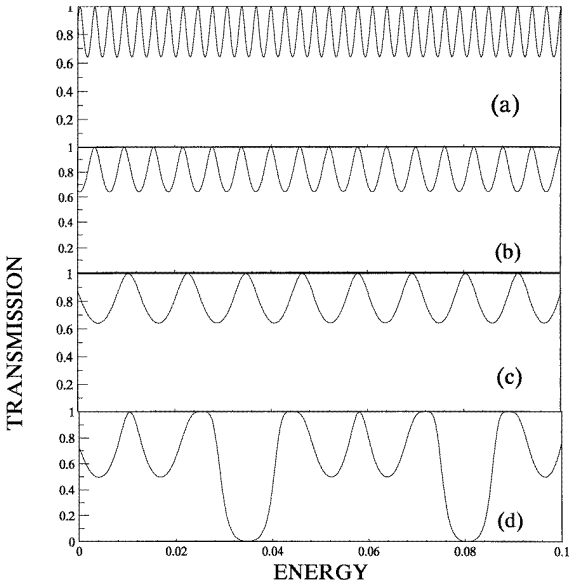

Figure 10. The comparison of electronic transmission via singly and doubly connected AB rings. (a) and (b) are for singly connected AB rings with chain lengths equal to 2000 and 1000, respectively; (c) and (d) are for doubly connected AB rings, where each arm segment length is equal to 1000 and the rung lengths are 0 and 1000, respectively.

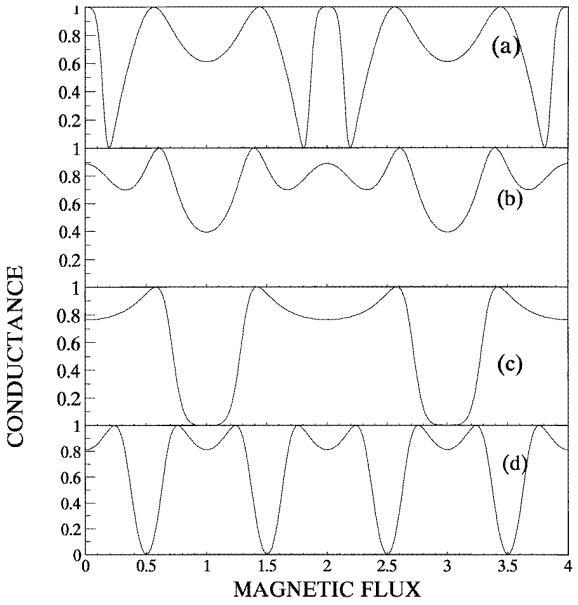

Figure 11. The conductance versus the magnetic flux for the doubly connected AB ring with length segments equal to 1000 and the incident-electron energy fixed at 1.1. The rung length is chosen as (a) 1000, (b) 500, and (c) 0, and (d) is for an ordinary AB ring with chain lengths 2000.

length of a doubly connected structure; for zero rung length, a doubly connected ring simply reduces to two attached singly connected rings. In figure 11 we show the conductance oscillations as a function of the magnetic flux with rung length variations. In both cases the curves show periodic magneto-oscillations governed by strong field dependence, and the patterns can be modulated by varying the rung length. Moreover, from figure 11(c) and figure 11(d) we observe many zero-transmission points inside the allowed band which could play a very special role in band engineering technology.

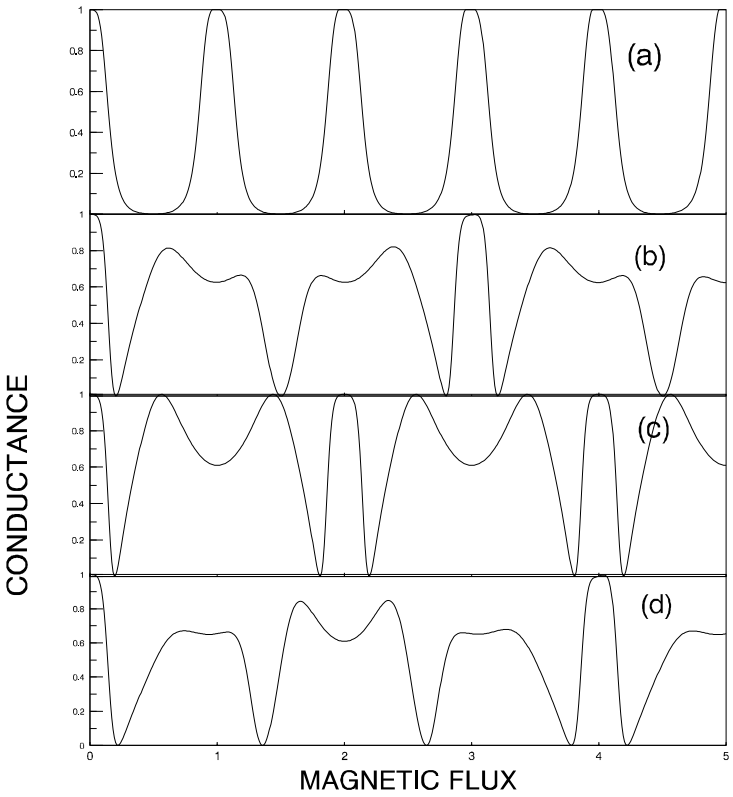

Figure 12. The conductance versus the magnetic flux for a doubly connected AB ring with different partitions of the magnetic flux; each arm segment is 1000 and the rung length is also 1000. (a) $\phi_2 = 0$, (b) $\phi_2 = \frac{1}{2}\phi_1$, (c) $\phi_2 = \phi_1$, and (d) $\phi_2 = 3\phi_1$.

A metal–insulator transition can be induced by varying the magnetic field strength, while the interference patterns obtained which show magneto-oscillation periodicities depend on the distribution of the magnetic flux between the closed paths. In figure 12 we show the electronic conductance for a doubly connected AB ring structure with magnetic flux periods (a) ϕ_0, (b) $3\phi_0$, (c) $2\phi_0$, and (d) $4\phi_0$. One can easily deduce the relation between the period of oscillation and the distribution of the magnetic fluxes, noticing that the phase shift for every chain must be an integer multiple of 2π. These results are consistent with those obtained for singly connected multi-arm rings [13].

4. Discussion

Mesoscopic systems provide the most elegant and instructive tool for the study of quantum mechanical interference phenomena of one-particle wave functions. In the case of multi-arm rings with single-channel leads, the electron waves incident from the left split and recombine at the exit with coherent multi-interference effects. The induced phase changes are not the same for different paths of propagation, which leads to rather complicated interference patterns. We find $t(-E) \neq t(E)$ for the transmission coefficient in the absence of magnetic fields when some chains consist of odd and others of even numbers of sites. The familiar condition $t(E) = t(-E)$, due to the electron–hole parity symmetry, is recovered only when the chain lengths are all even or all odd. Moreover, an averaged transmission enhancement is obtained for random chain lengths from the suppression of quantum interference. A single impurity in the structure is shown to modify the magnetoconductance oscillation pattern non-trivially, but its periodicity is maintained. Finally, we studied doubly connected AB rings exposing the differences from their singly connected counterparts. We show that the additional nodes present in doubly connected structures provide extra interference effects and transmission zeros for certain energies while $t(-E) = t(E)$ is satisfied. Moreover, we demonstrate how the conductance pattern can be modulated by varying an appropriately defined rung length in these structures.

Three types of oscillation are met in quantum transport via mesosopic AB rings. The magneto- and electro-oscillations have been studied by many authors, while the third kind, due to variations in the electron energy, are studied in the present paper. We also discuss the relationship between energy-induced and electro-oscillations, showing for singly connected structures with equal numbers of chains that the energy-induced oscillation period ϕ_E is the exact doubling of the voltage-induced oscillation period ϕ_V. Moreover, the energy-induced oscillation pattern shows many very sharp peaks when the number of chains in the structure considered increases. Structural variations are also expected to modify strongly the periodic magneto-oscillation curves.

In summary, we have studied the quantum transport properties of various topological mesoscopic ring structures joined at their ends to form ideal single-channel leads, with and without the presence of impurities. The band formation is analysed and compared with results for usual ordered singly connected systems, and we point out the essential differences. We also discuss a relationship between the periods of the energy- and voltage-induced oscillations, and display periodicity regularity for doubly connected AB rings. The results presented in this paper are expected to be useful for purposes of band tailoring and also for microelectronic device engineering.

Acknowledgments

This work was supported by the National Natural Science Foundation of China, a ΠΕΝΕΔ grant from the Greek Secretariat of Science and Technology, and a TMR programme of the EU.

References

[1] For reviews see
Altshuler B L, Lee P A and Webb R A (ed) 1991 *Mesoscopic Phenomena in Solids* (New York: North-Holland)
[2] Fukuyama H and Ando T 1992 *Transport Phenomena in Mesoscopic Systems* (Berlin: Springer)

[3] Washburn S and Webb R A 1992 *Rep. Prog. Phys.* **55** 1311
[4] Capasso F and Datta S 1990 *Phys. Today* **43** (2) 74
[5] Datta S 1989 *Superlatt. Microstruct.* **6** 83
[6] Sols F, Macucci M, Ravaioli U and Hess K 1989 *J. Appl. Phys.* **66** 3892
[7] Deo P S and Jayannavar A M 1994 *Phys. Rev.* B **50** 11 629
[8] Büttiker M, Imry Y and Azbel M Ya 1984 *Phys. Rev.* A **30** 1982
[9] Matteucci G and Pozzi G 1985 *Phys. Rev. Lett.* **54** 2469
[10] Webb R A, Washburn S, Umbach C P and Laibowitz R B 1985 *Phys. Rev. Lett.* **54** 2696
[11] Peshkin M and Tonomura A 1990 *The Aharonov–Bohm Effect* (Berlin: Springer)
[12] Gefen Y, Imry Y and Azbel M Y 1984 *Phys. Rev. Lett.* **52** 129
[13] Chen Y, Xiong S J and Evangelou S N 1997 *Phys. Rev.* B **56** 4778
[14] Xia J B 1992 *Phys. Rev.* B **45** 3593
[15] Landauer R 1957 *IBM J. Res. Dev.* **1** 223
Landauer R 1970 *Phil. Mag.* **21** 863
Büttiker M 1986 *Phys. Rev. Lett.* **57** 1761
[16] Wu C H and Mahler G 1991 *Phys. Rev.* B **43** 5012
[17] Takai D and Ohta K 1993 *Phys. Rev.* B **48** 1537
Takai D and Ohta K 1994 *Phys. Rev.* B **50** 2685